Eur. Phys. J. D **8**, 287–297 (2000)

THE EUROPEAN PHYSICAL JOURNAL D

EDP Sciences

The influence of mode coupling on the non-linear evolution of tearing modes

M.F.F. Nave[1,2], R. Coelho[2], E. Lazzaro[3,a], and F. Serra[2]

[1] JET Joint Undertaking, Abingdon, Oxfordshire OX14 3EA, UK
[2] Associação EURATOM/IST, Instituto Superior Tecnico, 1096 Lisboa Codex, Portugal
[3] Istituto di Fisica del Plasma del CNR "P. Caldirola", Assoc. EURATOM-ENEA-CNR, via R. Cozzi 53, 20125 Milan, Italy

Received 4 May 1999 and Received in final form 23 July 1999

Abstract. On the basis of tearing mode theory a simple but physically explicit model of the evolution of toroidally coupled rotating magnetic islands has been developed. The basic mechanism identified by the model in the island evolution is the locking in phase of rotating islands that leads to rapid destabilisation of an initially stable mode. Destabilisation of marginally stable (2, 1) and (3, 1) modes is analysed in several scenarios. It is shown that mode coupling is an effective way of destabilising a $m = 3$ island in a low-β plasma. The numerical examples presented show the individual roles of coupling, inertia and a resistive wall. The model was applied for the analysis of MHD observations of an ASDEX discharge.

PACS. 52.35.Py Plasma macroinstabilities (hydromagnetic, e.g., kink, fire-hose, mirror, ballooning, tearing, trapped-particle, flute, Rayleigh-Taylor, etc.)

1 Introduction

Magnetic islands, observed in many Tokamak discharges, are associated with global stability and are believed to influence energy confinement, although the general problem of their role on transport is still open [1]. The understanding of how rotating islands evolve and interact with the plasma and surrounding vessel is of great importance in the avoidance of locked modes and disruptions, which are both key issues for a thermonuclear fusion reactor.

The conditions of stability for modes of different helicity coupled by toroidal, shaping and finite pressure effects were developed analytically in first order approximation by Connor *et al.* [2,3]. Stability analysis in toroidal geometry can also be obtained with a variety of linear full-magnetohydrodynamic (MHD) codes [4]. These very complete models focus on the conditions of stability of the interacting modes, but have not yet been used to display the full temporal evolution. Computational non-linear evolution of modes in toroidal geometry has been addressed by Carreras *et al.* [5]. Although in principle both linear and non-linear codes can be adapted to study the numerical evolution of coupled modes, they would not provide simple analytic terms for inclusion in the present studies of feedback stabilisation developed in cylindrical geometry [6–9].

In order to study the evolution of amplitude and rotation of coupled tearing modes, an alternative simpler approach is considered here. The evolution of two coupled modes is treated by analogy with the problem of a single mode driven by external electro-dynamic fields. This similarity has been noted in reference [6].

The linear stability properties of modes depend sensitively on drift effects in a finite pressure plasma. However, beyond the linear stage, finite islands subject to external electro-dynamic fields enter a non-linear driven regime where the density, temperature (or pressure) gradients which determine the drift frequencies tend to be flattened and the mode frequency is determined by the dominating external torques.

A full consideration of Tokamak geometry on (m, n) mode coupling implies inclusion of finite pressure and flux surface shaping effects, in addition to toroidal ones. However an essential feature of the toroidal geometry, surviving even in the $\beta = 0$ limit and circular cross-section torus, is the appearance of coupling with side-band harmonics modes. Thus the electro-dynamic coupling can, quite generally, be represented for any given mode as the effect of suitable "external" current distribution, provided one can relate the phase and magnitude of the "effective" currents to the amplitude and phase of the side-band modes coupled to the mode under consideration. Unlike the problem of feedback stabilisation by an external current, in the study of coupling of a (m, n) mode with a ($m \pm 1$, n) mode, a current sheet of helicity ($m \pm 1$, n) is located inside the plasma.

In this paper, we consider contributions to the stability parameter Δ' coming from the (m, n) eddy currents

[a] e-mail: lazzaro@ifp.mi.cnr.it

excited in the resistive wall and from the internal time varying current sheets located on the surfaces where the side-band harmonics are resonant. A full-time derivative of the island angular momentum is taken into account, along the lines of reference [9]. We consider resistive modes with poloidal mode numbers $m > 1$ (a similar approach applied for the study of the coupling of the $m = 1$ and $m = 2$ harmonics can be found in [10]). Having determined the complex stability parameter for the (m, n) mode, suitable for a numerical solution, we will then adopt the approximation of neglecting the effects of finite current density in the ideal MHD region in order to obtain simpler analytic expressions for the equations describing the time evolution of island width and rotation.

The model has been applied to the study of destabilisation of small islands. Simulations were also carried out for the analysis of MHD observations of an ASDEX Tokamak discharge.

2 Formulation of the problem

In the case of toroidal geometry, the magnetic perturbations δB related to magnetic islands with different poloidal and toroidal mode numbers (m, n) have not only a single (m, n) component, but also side band harmonics. Each mode evolves driven by its own free energy and by the effect of the electro-dynamic (magnetic) fields generated by other modes, considered as external sources. Therefore the prototype problem is the investigation of the interaction of a magnetic island with a time varying current sheet source with specified helicity (m, n), amplitude and phase, located within the plasma. The model is fully specified when the localised "source currents" are associated uniquely to the amplitude and phase of the interacting modes. The tearing mode equation for each mode (m, n) with inhomogeneous source terms is then solved in order to obtain the complex stability parameter Δ' which is subsequently used in a non-linear Rutherford type equation for island growth [11], associated with the momentum balance equation governing island rotation.

We adopt a notation appropriate for the large aspect ratio reduced MHD description [12]. A helical magnetic field perturbation eventually evolving into a "magnetic island" is expressed in terms of a helical flux function

$$\delta\mathbf{B} = \mathrm{Re}(\boldsymbol{\nabla} \times (\Psi_{mn}\mathbf{b}_{mn})) \tag{1}$$

where $\mathbf{b}_{mn}(nr/mR_0)\hat{\boldsymbol{\theta}} + \hat{\mathbf{z}}$ and $\Psi_{mn} = \Psi_{mn}(r)\,\mathrm{e}^{\mathrm{i}(m\theta - nz/R_0+\phi)}$. The width of the island

$$W = \sqrt{\frac{16R_0q^2(r_\mathrm{s})}{r_\mathrm{s}Bq'(r_\mathrm{s})}\Psi_{mn}(r_\mathrm{s})} \tag{2}$$

is related to the amplitude of Ψ at the rational flux surface $q(r)$ (defined as $q(r) = rB/R_0B_\theta$, where R_0 is the Tokamak major radius and r the radius of the magnetic surface). The phase of the mode ϕ is such that $\mathrm{d}\phi/\mathrm{d}t = \omega$, ω being the mode frequency.

The linear tearing mode equation for Ψ_{mn} is written in our notation as

$$-\frac{B_\theta}{\mu_0 rB}\nabla_*^2\Psi_{mn}(m - nq) + \frac{m}{r}\lambda_0'\Psi_{mn} = 0 \tag{3}$$

where $\lambda_0' = \mathrm{d}/\mathrm{d}r(J_{0\|}/B)$, $\nabla_*^2 \equiv \nabla_\perp^2$ perpendicular to $\hat{\mathbf{z}}$ and $J_{0\|}$ is the equilibrium current density directed along the magnetic field. The stability parameter obtained from the solution of (3) in the vicinity of the singular point $r = r_\mathrm{s}$ is defined as

$$\Delta'\Psi_{mn}(r_\mathrm{s}) = \Psi'_{mn}(r_{\mathrm{s}+}) - \Psi'_{mn}(r_{\mathrm{r}-}). \tag{4}$$

The evolution of the width and rotation frequency of a magnetic island are a consequence of Faraday-Ohm's law and the current continuity equation. The key role in the growth and rotation of an island of mode numbers (m, n) is held by the stability parameter Δ' which describes the presence of a current sheet at the resonant surface where $q(r) = m/n$.

The real part of Δ' governs the island growth. In its non-linear stage the time evolution of the island width is well described by Rutherford's expression, as given in reference [11]

$$\frac{\mathrm{d}W}{\mathrm{d}t} = 1.16\frac{Z_\mathrm{eff}\eta}{\mu_0}\mathrm{Re}(\Delta'), \tag{5}$$

where Z_eff is the plasma effective charge and η is the Spitzer resistivity.

The imaginary part of Δ' gives the electromagnetic torque on the island defined as

$$T_\phi = \frac{8\pi^2R_0}{4\mu_0}nr_\mathrm{s}\mathrm{Im}(\Psi_{mn}^2(r_\mathrm{s})\Delta'). \tag{6}$$

The effective toroidal moment of inertia of the amount of plasma associated with an island of separatrix width (W) and mode numbers (m, n) is given by

$$I_\phi = \lambda^{(m)}nm_\mathrm{p}r_mR_0^3W_m \tag{7}$$

where n is the plasma density, m_p the proton mass and $\lambda^{(m)}$ is a geometric factor. The magnetic island, moving in the toroidal direction with a angular velocity equal to ω/n, will be accelerated or decelerated by this torque. In this work we consider valid the regime where the poloidal rotation is efficiently damped [13] by the poloidal projection of the parallel viscous stress, $\langle B_\theta\mathbf{e}_\theta \cdot \nabla \cdot \boldsymbol{\Pi}_{\|}\rangle \cong -nm_\mathrm{i}\nu_\mathrm{ii}\mu_\mathrm{li}V_\theta\langle B^2\rangle$ which dominates the other driving forces. Here ν_ii, μ_li are the ion-ion collision frequency and a viscosity coefficient according to the definitions of reference [13]. Consequently poloidal rotation is neglected and the role of viscosity is essentially that of allowing relative motion (toroidally) of the island with the ambient plasma.

In the absence of any torque, inertia will slow down a growing island in order to conserve angular momentum. Including these two sources the frequency of the mode will evolve in time according to

$$\frac{\mathrm{d}\omega}{\mathrm{d}t} = \frac{1}{I_\phi}\left[\frac{n}{R_0}T_\phi - \omega\frac{\mathrm{d}I_\phi}{\mathrm{d}t}\right]. \tag{8}$$

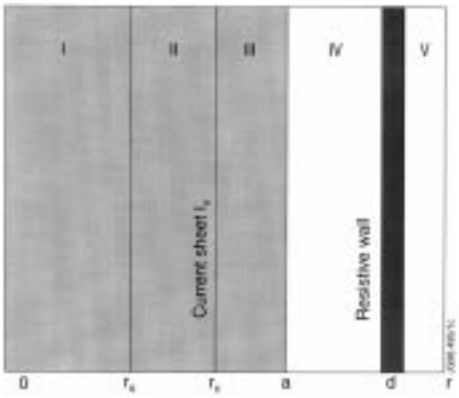

Fig. 1. Various regions where the flux function needs to be determined.

The simplest picture is obtained by solving the tearing mode equation (3) for the mode $(m,\ n)$ localised at $r_{\rm s}$, with the addition of a source term within the plasma with a current sheet $I_{\rm v} = I\exp[{\rm i}(m\theta - nz/R_0 + \phi_{\rm c})]$ placed at $r = r_{\rm c}$ and a resistive wall at $r = d$ (see Fig. 1). The solution of (3) is obtained by the method of variation of parameters and it is matched across the different regions shown in the Figure 1.

The solution of (3) in the different regions is of the form, developed in reference [8]:

$$\begin{aligned}
&\Psi_{\rm I} = \Psi_{\rm s}F_{0+}(r) && 0 \le r \le r_{\rm s}\\
&\Psi_{\rm II} = C^+_{\rm II}F_+(r) + C^-_{\rm II}F_-(r) && r_{\rm s} < r \le r_{\rm c}\\
&\Psi_{\rm III} = C^+_{\rm III}F_+(r) + C^-_{\rm III}F_-(r) && r_{\rm c} < r \le a\\
&\Psi_{\rm IV} = C^+_{\rm IV}(r/d)^{+m} C^-_{\rm IV}(r/d)^{-m} && a < r \le d\\
&\Psi_{\rm V} = C_{\rm w}(t)(r/d)^{-m} && d < r
\end{aligned} \qquad (9)$$

where F_{0+}, $F_\pm$ are dimensionless basic solutions of the tearing equation without source terms (internal or external currents, wall, etc.) which satisfy the boundary conditions

$$\begin{aligned}
&F_{0+}(r_{\rm s}) = F_-(r_{\rm s}) = F_+(r_{\rm s}) = 1\\
&\text{and}\quad F'_+(a) = m/aF_+(a);\quad F'_-(a) = -m/aF_-(a).
\end{aligned}$$

Across the resistive wall we use a constant Ψ approximation, valid for a thin wall [8,14], *i.e.* $\delta_{\rm wall}/d \ll 1/\tau_{\rm wall}\omega$, where $\delta_{\rm wall}$ is the thickness of the wall and $\tau_{\rm wall} = \mu_0\sigma_{\rm wall}\delta_{\rm wall}r_{\rm wall}/2$ is the vessel resistive time.

Imposing at $r_{\rm c}$, a and d the matching conditions to Ψ and the jump conditions of the type $[\Psi']_{r_{\rm c}} = \mu_0 I_{\rm v}/mr_{\rm c}$ on the derivative [8], we obtain for regions I and II:

$$\Psi_{\rm I} = \Psi_{\rm s}F_{0+}(r) \qquad (10)$$

$$\begin{aligned}
\Psi_{\rm II} = {}& \Psi_{\rm s}F_-(r) - I^-[F_+(r) - F_-(r)]\\
&- \left(\frac{a}{d}\right)^m \frac{(g - \hat{D}[g])}{f_{a,d}}\frac{[F_+(r) - F_-(r)]}{F_+(a)}{\rm e}^{-{\rm i}\phi}
\end{aligned} \qquad (11)$$

where $I^\pm = (\mu_0 I/r_{\rm c})(F_\pm(r_{\rm c})/\hat{W}[F_+, F_-]_{r_{\rm c}}){\rm e}^{{\rm i}(\phi_{\rm c}-\phi)}$ appears from the use of the method of variation of parameters ("$\hat{W}$" stands for the Wronskian of the two functions),

$$\begin{aligned}
g(t) &= [\Psi_{\rm s} - I^+ + I^-]\left(\frac{a}{d}\right)^m F_-(a){\rm e}^{{\rm i}\phi},\\
f_{a,r} &= 1 - \left(\frac{a}{d}\right)^{2m}\frac{F_-(a)}{F_+(a)},\\
\hat{D}[g(t)] &= \frac{1}{\tau_{\rm w}}\int_{-\infty}^{t} g(t'){\rm e}^{\frac{t'-t}{\tau_{\rm w}}}{\rm d}t',\\
\tau_{\rm w} &= \frac{\tau_{\rm wall}}{m}f_{a,d}.
\end{aligned}$$

The complex stability parameter is then given by the evaluation at $r_{\rm s}$ of the expression

$$\begin{aligned}
\Delta' = {}& [F'_+(r_{\rm s}) - F'_-(r_{\rm s})] - \frac{I^-}{\Psi_{\rm s}}[F'_+(r_{\rm s} - F_-(r_{\rm s})]\\
&- \left(\frac{a}{d}\right)^m \frac{(g - \hat{D}[g])}{f_{a,d}}\frac{[F'_+(r_{\rm s}) - F'_-(r_{\rm s})]}{\Psi_{\rm s}F_+(a)}{\rm e}^{-{\rm i}\phi}.
\end{aligned} \qquad (12)$$

The first term on the right hand side of (12) is the natural stability parameter for the mode $(m,\ n)$, Δ'_0, in the absence of sources (for islands larger than the resistive layer, Δ'_0, is a function of the island width, but does not depend on the mode frequency). The second term gives the contribution from the current sheet, while the third term is the contribution from the wall.

Expression (12) supplies a rigorous stability parameter, expressed in terms of calculated solutions of the tearing mode equation for the mode $(m,\ n)$ without any sources. It is instructive however, to gain a physical insight into the mechanism of coupling, by writing the coupling coefficients in the "tenuous plasma" approximation where the current density effects in the ideal MHD region (far from the reconnecting layer) are neglected and $F_\pm(r) \cong (r/r_{\rm s})^{\pm m}$. This leads to $\hat{W}[F_+, F_-]_{r_{\rm c}} = -2m/r_{\rm c}$; $F'_+ - F'_- = 2m/r_{\rm s}$ and $f_{a,d} \approx 1$; and to leading order we obtain

$$\begin{aligned}
\Delta'_m = {}& \Delta'_0 + \frac{\mu_0 I}{\Psi_{\rm s}}\frac{1}{r_{\rm s}}\left(\frac{r_{\rm s}}{r_{\rm c}}\right)^{m(m\pm1-m)}{\rm e}^{{\rm i}(\phi_{\rm c}-\phi)}\\
&- \frac{2m}{r_{\rm s}}\left(\frac{r_{\rm s}}{d}\right)^{2m}\frac{(\omega_m\tau_{\rm wm})^2 + {\rm i}(\omega_m\tau_{\rm wm})}{1 + (\omega_m\tau_{\rm wm})^2},
\end{aligned} \qquad (13)$$

where the exponent $m \pm 1$ indicates the interaction of the mode $m,\ n$ with either an internal $(m-1),\ n$ or an external $(m+1),\ n$ harmonic.

From expressions (5, 8, 13), equations for the temporal evolution of the island width and frequency can be obtained as a function of the applied current I and the phase difference $(\phi_{\rm c} - \phi)$. Given that our goal is to obtain equations describing the coupling between two modes $(m,\ n)$ and $(m \pm 1,\ n)$, the next step will be to write the applied current I as a function of the magnitude of the $(m \pm 1,\ n)$ magnetic perturbation. The phase difference $(\phi_{\rm c} - \phi)$ will naturally become the phase difference between the two modes $(\phi_{m\pm1,n} - \phi_{m,n})$. The conservation of the total torque of our system based on two modes

and a conducting wall will provide the means of determining the equivalent complex stability parameter for the $(m\pm1, n)$ mode. In the next section we will derive the stability parameters of the two coupled (m, n) and $(m\pm1, n)$ modes and subsequently the equations for the time evolution of island width and frequency.

3 The non-linear model including mode coupling

In toroidal geometry the magnetic flux perturbation will have a main helicity and a series of side-band harmonics arising from the dependence on the toroidal helical coordinate χ^* as shown in reference [15]:

$$\Psi_{mn}(r,\theta,\varphi) = \Psi_{mn}(r)\cos m\chi^*, \tag{14}$$

where

$$m\chi^* = m(\theta - \lambda\sin\theta) - n\varphi$$

$$\text{and} \qquad \lambda = \frac{r_\mathrm{s}}{R_0}\left[1+\beta_\mathrm{p}+\frac{l\mathrm{i}}{2}\right].$$

From now on the label "n" will be dropped. The $(m,\ n)$ side-band harmonic associated to a $(m\pm1)$ magnetic island (modelled by a localised helical current) has a radial dependence given by

$$\Psi^{(m)}_{(m\pm1)} = (m\pm1)\Psi_{(m\pm1)}\varepsilon_\mathrm{s}^m\frac{r_{\mathrm{s}(m\pm1)}}{2mR_0} \tag{15}$$

where $\varepsilon_\mathrm{s} \cong \min(r_{\mathrm{s}(m\pm1)}/r, r/r_{\mathrm{s}(m\pm1)})$.

One may observe that the magnitude of the $(m,\ n)$ harmonic of the $m\pm1$ mode is already a function of the $m\pm1$ island width ($W_{m\pm1} = const\sqrt{\Psi_{(m\pm1)}}$). Imposing the matching condition

$$\frac{\mathrm{d}}{\mathrm{d}r}\Psi^{(m)}(r_{\mathrm{s}(m\pm1)+}) - \frac{\mathrm{d}}{\mathrm{d}r}\Psi^{(m)}(r_{\mathrm{s}(m\pm1)-}) = -\frac{\mu_0 I}{r_{\mathrm{s}(m\pm1)}}$$

one can obtain:

$$I = \frac{1}{\mu_0}\frac{r_{\mathrm{s}(m\pm1)}}{R_0}(m\pm1)\Psi_{\mathrm{s}(m\pm1)}, \tag{16}$$

which can also be derived from a full toroidal non-linear MHD formulation as in reference [5].

Then the stability parameter for the m mode containing contributions from coupling and the resistive wall is given as

$$\begin{aligned}\Delta'_m = \Delta'_{0(m)} &+ \frac{(m\pm1)}{R_0}\frac{r_{\mathrm{s}(m\pm1)}}{r_{sm}}\left(\frac{r_{sm}}{r_{\mathrm{s}(m\pm1)}}\right)^{m(m\pm1-m)} \\ &\times \frac{\Psi_{\mathrm{s}(m\pm1)}}{\Psi_{sm}}\mathrm{e}^{\mathrm{i}(\phi_{m\pm1}-\phi_m)} \\ &- \frac{2M}{r_{sm}}\left(\frac{r_{sm}}{d}\right)^{2m}\frac{(\omega_m\tau_{\mathrm{wm}})^2 + \mathrm{i}(\omega_m\tau_{\mathrm{wm}})}{1+(\omega_m\tau_{\mathrm{wm}})^2}\,.\end{aligned} \tag{17}$$

The torque on the m island arising from the imaginary part of the wall term finds its counterpart on a torque applied to the conducting vessel due to the time varying magnetic perturbation penetrating the wall. In order to maintain global torque balance in the system, there must be a suitable "coupling" term in the stability parameter of the $m\pm1$ island. Moreover, one can easily conclude that this term should be a function of the amplitudes and phases of the two modes of the form

$$\Delta'_{\mathrm{coup}(m\pm1)} = const\frac{\Psi_{sm}}{\Psi_{\mathrm{s}(m\pm1)}}\mathrm{e}^{\mathrm{i}(\phi_m-\phi_{m\pm1})}. \tag{18}$$

The coupling coefficient (a single parameter) can be obtained considering that the system is initially in mechanical equilibrium and that the perturbations do not apply any net torque. Thus the stability parameter of the $m\pm1$ island has a similar structure to expression (17).

We can then obtain the following dynamic system of equations for the description of the time evolution of the island width and mode frequency

see following equations

$$\begin{aligned}\frac{\mathrm{d}W_m}{\mathrm{d}t} = 1.16\frac{Z_\mathrm{eff}\eta_m}{\mu_0}\Bigg[&\Delta'_m + \frac{(m\pm1)}{R_0}\frac{r_{\mathrm{s}(m\pm1)}}{r_{sm}}\left(\frac{r_{sm}}{r_{\mathrm{s}(m+1)}}\right)^{m(m\pm1-m)}\frac{k_{m\pm1}W^2_{m\pm1}}{k_m W^2_m}\cos(\phi_{m\pm1}-\phi_m) \\ &- \frac{2m}{r_{sm}}\left(\frac{r_{sm}}{d}\right)^{2m}\frac{(\omega_m\tau_{\mathrm{wm}})^2}{1+(\omega_m\tau_{\mathrm{wm}})^2}\Bigg]\end{aligned} \tag{19}$$

$$\begin{aligned}\frac{\mathrm{d}\omega_m}{\mathrm{d}t} = \frac{1}{I^{(m)}_\phi}\Bigg[&\frac{2\pi^2 n^2 r_{sm}R_0}{\mu_0}\Bigg(\frac{(m\pm1)}{R_0}\frac{r_{\mathrm{s}(m\pm1)}}{r_{sm}}\left(\frac{r_{sm}}{r_{\mathrm{s}(m\pm1)}}\right)^{m(m\pm1-m)} k_m k_{m\pm1}W^2_m W^2_{m\pm1}\sin(\phi_{m\pm1}-\phi_m) \\ &- \frac{2m}{r_{sm}}\left(\frac{r_{sm}}{d}\right)^{2m}\frac{(\omega_m\tau_{\mathrm{wm}})}{1+(\omega_m\tau_{\mathrm{wm}})^2}k^2_m W^4_m\Bigg) - \omega_m\frac{\mathrm{d}I^{(m)}_\phi}{\mathrm{d}t}\Bigg]\end{aligned} \tag{20}$$

$$\frac{\mathrm{d}W_{m\pm1}}{\mathrm{d}t} = 1.16\frac{Z_{\mathrm{eff}}\eta_{m\pm1}}{\mu_0}\left[\Delta'_{(m\pm1)} + \frac{(m\pm1)}{R_0}\left(\frac{r_{sm}}{r_{s(m\pm1)}}\right)^{m(m\pm1-m)}\frac{k_m W_m^2}{k_{m\pm1}W_{m\pm1}^2}\cos(\phi_m-\phi_{m\pm1}) - \frac{2(m\pm1)}{r_{s(m\pm1)}}\left(\frac{r_{s(m\pm1)}}{d}\right)^{2(m\pm1)}\frac{(\omega_{m\pm1}\tau_{w(m\pm1)})^2}{1+(\omega_{m\pm1}\tau_{w(m\pm1)})^2}\right] \quad (21)$$

$$\frac{\mathrm{d}\omega_{m\pm1}}{\mathrm{d}t} = \frac{1}{I_\phi^{(m\pm1)}}\left[\frac{2\pi^2 n_{m\pm1}^2 r_{s(m\pm1)}R_0}{\mu_0}\left(\frac{(m\pm1)}{R_0}\left(\frac{r_{sm}}{r_{s(m\pm1)}}\right)^{m(m\pm1-m)}k_m k_{m\pm1}W_m^2W_{m\pm1}^2\sin(\phi_m-\phi_{m\pm1}) - \frac{2(m\pm1)}{r_{s(m\pm1)}}\left(\frac{r_{s(m\pm1)}}{d}\right)^{2(m\pm1)}\frac{(\omega_{m\pm1}\tau_{w(m\pm1)})}{1+(\omega_{m\pm1}\tau_{w(m\pm1)})^2}k_{m\pm1}^2W_{m\pm1}^4\right) - \omega_{m\pm1}\frac{\mathrm{d}I_\phi^{(m\pm1)}}{\mathrm{d}t}\right] \quad (22)$$

where $\Psi_{sm} = k_m W_m^2$ and $\Psi_{s(m\pm1)} = k_{m\pm1}W_{m\pm1}^2$.

The set of equations (19–22) show the role and competition of the coupling mechanism with the inertia and the resistive wall effects (N.B. the subscript "o" has been dropped from the natural stability parameter, which from now on will be indicated as Δ'). Island stability will depend on the initial conditions, and in a complex way on the relative amplitude of the various terms, as it will be shown in the examples below. In the growth equations for W (19, 21) the coupling term (second term) is an increasing function of the other island width. Coupling may have either a stabilising or destabilising effect depending on the difference of phase. The evolution of the phase difference is essential in the determination of island growth stability and, it will depend on the coupling as well as on the effect of the resistive wall and plasma inertia terms on island rotation.

In the equations for the evolution of the mode frequency (20, 22) the driving torque (first term) is due to the coupling with the other island, while the second and third terms represent the resistive wall braking and the inertia. The toroidal momentum of inertia $I_\phi \propto W$, contributes to accelerating or slowing down the island rotation frequency, depending on whether the island width is decreasing or increasing.

A full treatment of the problem of rotating islands should also include viscosity. Here, we have chosen to consider a low viscosity regime, since our main object in this paper is to discuss the role of the electro-dynamic coupling. The inertial force should be compared with that of the viscous force that couples the island rotation to the surrounding plasma and tends to restore rotation at the natural frequency ω_0 determined by the plasma conditions. The ratio of the viscous force on an island can be estimated as $\xi = (W/r_s)(\tau_v/\tau_\omega)$, where τ_ω is the relevant time scale of variation of the frequency and τ_v the (anomalous) perpendicular viscous damping time scale. For values of $\tau_\omega < \tau_v(W/r_s)$, inertial effects prevail over viscous ones. This can occur for relatively large islands $W/r_s \sim 10^{-1}$ and the typical estimate of $\tau_v \sim \tau_E$, the energy confinement time.

4 Stability of coupled m = 2 and m = 3 tearing modes

In this section, we illustrate the proprieties of the above model by making a study of the stability of coupled $m = 2$ and $m = 3$ modes with toroidal mode number $n = 1$. We start by showing the effect of coupling on two marginally stable modes, both in rotating and non-rotating scenarios. Stability depends on the competition of the various terms in equations (20–23) which will be introduced one by one for added clarity.

In all numerical simulations we have taken a parabolic j profile $j = j_0(1-x^2)^2$, where $x = r/a$, with the resonant surfaces at $r_{s2}/a = 0.74$, $r_{s3}/a = 0.95$, and aspect ratio $\varepsilon = 4$. The moment of inertia is calculated for a plasma with a parabolic density profile, $n = n_0(1-x^2)$ with central density $n_0 = 5\times10^{19}$ m^{-3}, while for the wall we use $a/d = 0.7$ and $\tau_{wall} = 15$ ms. These parameters are relevant for the ASDEX experimental results discussed in Section 5. Here for simplicity we take the constant $Z_{\mathrm{eff}}\eta/\mu_0$, which appear in the equations for $\mathrm{d}W/\mathrm{d}t$, to be the same for both modes. Proper experimental radial profiles are considered in Section 5.

4.1 The effect of coupling on island growth

In order to illustrate the effect of coupling on the stability of magnetic islands, we start by considering a simple case where the natural Δ' and the wall terms are neglected. It should be noted that the instability index Δ' is indeed a non-linear function of the island width W, which eventually gives a contribution to the island evolution. However this is a result of the feedback to the background plasma profiles, which cannot be included in the simple model we consider presently for the definite purpose of investigating a regime of dominating toroidal coupling.

First we consider the effect of coupling on island growth when the two marginally stable islands do not rotate. The evolution of the island widths is simply

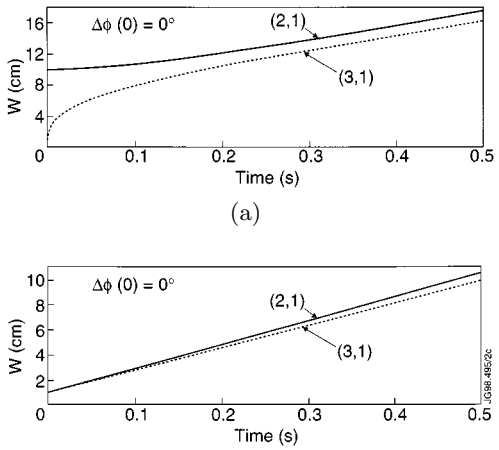

Fig. 2. The effect of coupling on marginally stable, non-rotating islands. For $\Delta\phi = 0$ mode coupling makes both modes unstable.

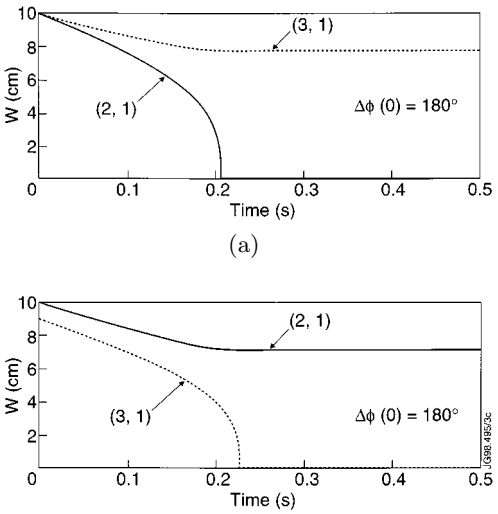

Fig. 3. With $\Delta\phi = \pi$, stability for both modes increase (in order to avoid a divergent solution, W was not allowed to decrease below 0.1 cm).

given by

$$\frac{\mathrm{d}W_2}{\mathrm{d}t} = c_2 \frac{W_3^2}{W_2^2} \cos\Delta\phi, \tag{23}$$

$$\frac{\mathrm{d}W_3}{\mathrm{d}t} = c_3 \frac{W_2^2}{W_3^2} \cos\Delta\phi. \tag{24}$$

Thus for any given phase difference, $\Delta\phi = \phi_3 - \phi_2$, the island widths evolve in accord with the relation $W_3^5(t) - W_3^5(0) = (9/4)(x_2^3/x_3^3)(s_2^2/s_3^2)\{W_2^5(t) - W_2^5(0)\}$, which shows that island growth is determined by the ratio of the initial island sizes, and by the relative position of the two rational surfaces and shear (defined as $s = (1/q)(\mathrm{d}q/\mathrm{d}x)$).

Clearly, stability for both modes depend on the sign of the phase difference, such that both islands are nonlinearly unstable when $0 \leq |\Delta\phi| < \pi/2$. The simulations in Figures 2 and 3 show cases with fixed phase differences $\Delta\phi = 0$ and $\Delta\phi = \pi$, respectively.

When $\Delta\phi = 0$, coupling makes both modes nonlinearly unstable, independent of their initial sizes. This is shown in Figure 2a for initially identical island sizes and, in Figure 2b for an $m = 2$ island initially one order of magnitude larger than the $m = 3$ island. In the latter, the larger coupling term for the $m = 3$ island brings its width to a size comparable to the width of the $m = 2$ in ~ 200 ms. It can be easily perceived that, asymptotically, the coupling leads to an equal growth of both islands. Therefore, the width of the (3, 1) island will ultimately evolve parallel to the (2, 1) island width. Depending on the constants, the (3, 1) island may evolve into a size larger than the (2, 1).

Figure 3 shows that when $\Delta\phi = \pi$, stability for both modes increase. In Figure 3a where the two modes have initially identical widths, the $m = 2$ mode decreases in size faster than the $m = 3$. In Figure 3b a small offset in the initial island sizes reverses this result, with the $m = 3$ decreasing in size, while the $m = 2$ remains marginally stable. The bifurcation point corresponds to the condition

$$\frac{\mathrm{d}^2W_2}{\mathrm{d}t^2} = \frac{\mathrm{d}^2W_3}{\mathrm{d}t^2} = 0,$$

leading to a critical (2, 1) island width given by

$$W_2|_{\mathrm{crit}} = \left[\frac{4}{9}\frac{x_3^3}{x_2^3}\frac{s_3^2}{s_2^2}\right]^{1/5} W_3.$$

4.2 Phase locking

In the two previous examples the two modes were kept at rest. However in practice this is not possible since even if the wall is neglected, the phases will change due to the effects of coupling and inertia. Coupling on its own makes both modes oscillate around an average frequency.

Figure 4 shows an example with similar initial conditions to the ones in Figure 2a, *i.e.* $W_2(0) = W_3(0)$ and $\omega_2(0) = \omega_3(0) = 0$. However, the frequency is now allowed to evolve, with the inertia term on average one order of magnitude smaller than the electromagnetic torque due to the coupling. The initial phase difference is $\Delta\phi(0) = \pi/2$, thus the initial coupling on the island sizes is zero. Both island sizes remain nearly unchanged in the initial 5 ms. On the other hand, the difference of phase changes due to the non-null electromagnetic torque. At zero phase difference both islands become unstable. Island growth continues until the phase difference goes through an extremum value and a new period of marginal stability starts. The dominant coupling torque ensures that the phase difference on average locks to zero, which is an unstable situation, thus the overall effect is that of both islands on average increasing in size similarly to the example shown

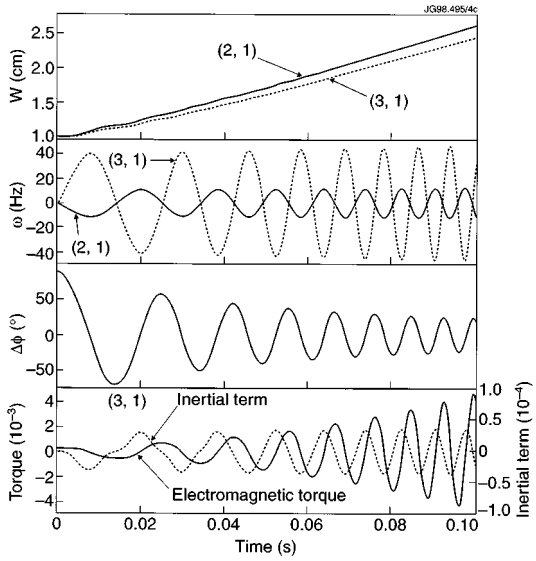

Fig. 4. The effect of coupling on marginally stable modes with initial $\omega(0) = 0$ and $\Delta\phi = \pi/2$.

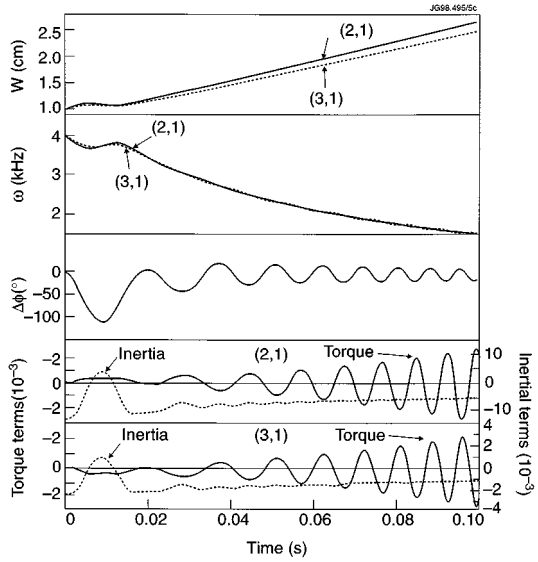

Fig. 5. The effect of coupling on marginally stable modes with initial $\omega(0) = 4$ kHz and $\Delta\phi = 0$.

in Figure 2a, while the frequencies oscillate around zero (N.B. in all figures given below the frequency is expressed in cycles/s).

A large initial frequency, such that the inertia term in the equation for the frequency is dominant, enforces marginal stability for a longer period of time. The simulation in Figure 5, shows that while the initial frequencies are large, both islands are kept marginally stable on average. This result holds independent of the initial value of the phase difference. In Figure 5, marginal stability is maintained until nearly 15 ms (even though we have started with the most unstable phase difference, *i.e.* $\Delta\phi(0) = 0$). As the mode frequency decreases and the electromagnetic torque starts to compete with inertia,

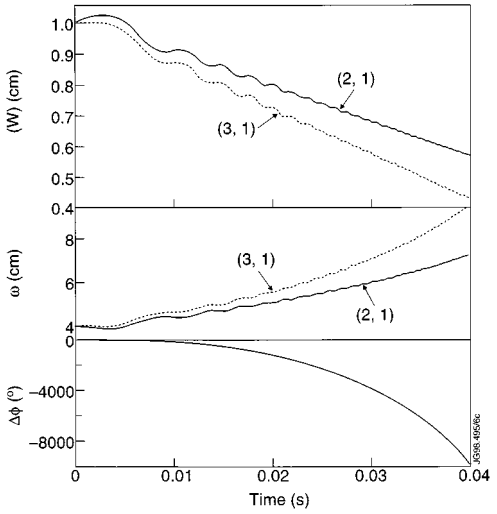

Fig. 6. As the example in Figure 5, but including the wall terms.

the phase difference once more, on average, locks to zero with the consequence that island stability is lost (again rendering the result of Fig. 2a).

Phase locking with $\Delta\phi = 0$ leads to frequency locking. In the absence of a wall (and neglecting the viscous drag), the average frequency is determined by the plasma inertia term. Then the average frequency evolves as

$$\omega(t) = \frac{\omega(0)W(0)}{W(t)} \,.$$

Differential rotation, *i.e.* $\omega_2(0) \neq \omega_3(0)$, and island sizes with initial different values, will change the time of phase locking, but overall will lead to similar results to those shown in Figures 4 and 5. An example with differential rotation is shown later in Section 5.

4.3 The effect of the wall

The stabilising and damping effects that the wall has on the growth and rotation of the modes, limit the achievement of a phase lock between the modes. For large frequencies, where the inertial term dominates the mode frequency evolution, different scenarios can be identified for $\Delta\phi(0) = 0$, where the islands may or not be destabilised according to the magnitude of the initial islands width.

First, when both island widths are small ($W/a \sim 10^{-2}$), phase lock does not occur since the stabilising effect of the wall weakens the coupling effect on the mode rotation. (This is shown in Fig. 6 for an input frequency, $\omega_2(0) = \omega_3(0) = 4$ kHz.) In this small island width limit, the electromagnetic torque arising both from the wall (relevant mainly for low frequencies) and from coupling are much smaller than the inertial contribution. On the other hand, if the initial island widths are increased to $W/a \geq 5 \times 10^{-1}$, increasing coupling, the general result obtained is the one where both islands are destabilised and phase lock is easily accomplished (as it will be shown below in the examples where all terms are included).

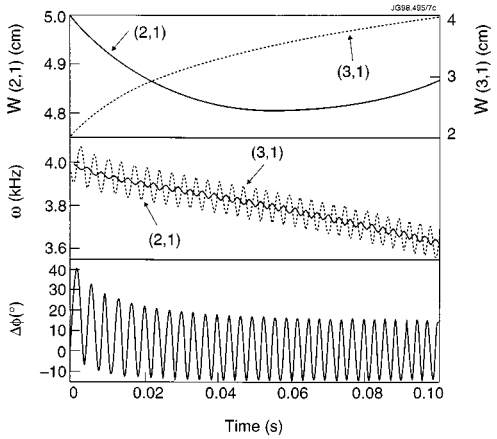

Fig. 7. Different initial island width scenario ($W_2(0) = 5$ cm, $W_3(0) = 2$ cm) showing a transient period where stabilisation of the (2, 1) island is accompanied by a decrease in frequency.

There is however a scenario worth mentioning, which is obtained when the initial island sizes are not identical, and one of the modes has a considerably larger island width. In Figure 7, we show the case where $W_2/a \geq 10^{-1}$, while $W_3/a \approx 5 \times 10^{-2}$. Since the magnitude of the coupling term in the rotation of both islands is now two orders of magnitude larger than in the example in Figure 6, phase locking occurs. However, in this case phase locking does not imply in an immediate loss of stability. Since the wall plays an important role in the stability of the (2, 1) mode, it allows for a transient period of around 60 ms where island stabilisation is maintained while the rotation frequency decreases. Due to the relative difference in the initial island widths, coupling is only marginally affecting the stability of the (2, 1) island. Up to here, we have neglected the natural stability parameter (*i.e.* we have taken $\Delta'_2 = \Delta'_3 = 0$). In many Tokamak situations, with parabolic-type j-profiles, $\Delta'_2 = 0$, while $\Delta'_3 \leq 0$. Below, we show a solution of equations (19–22) with all terms included. Numerical simulations were done for the case of $W_2/a \sim 5 \times 10^{-2}$ and $W_3/a \sim 10^{-2}$ for 3 different wall conditions, namely: a resistive wall, a perfectly conducting wall and a wall at infinity. The input frequency is $\omega_2(0) = \omega_3(0) = 4$ kHz and $\Delta\phi(0) = 0$ as in the previous two figures. The stability parameters $\Delta'_2(W)$ and $\Delta'_3(W)$ considered, are shown in Figure 8. These were obtained in a quasi-linear approximation from the solution of the tearing mode equation.

The results of the simulations are shown in Figure 9. Mode coupling ensures phase locking with the consequent destabilisation of the (3, 1) mode instability in just a few micro-seconds. The slow saturation of the $W(t)$ curves is controlled by $\Delta'_2(W)$. The average rotation frequency is controlled mostly by inertia, except at low frequencies in the resistive wall case, where both islands are brought to rest due to locking to the wall at $t = 170$ ms. In the other two cases the final frequency is determined by expression (26), *i.e.* the frequency tends asymptotically to a value $\omega_{\text{final}} \cong \omega(0)W(0)/W_2^{\text{sat}}$ (with $W_2^{\text{sat}} \sim 10$ cm in this example).

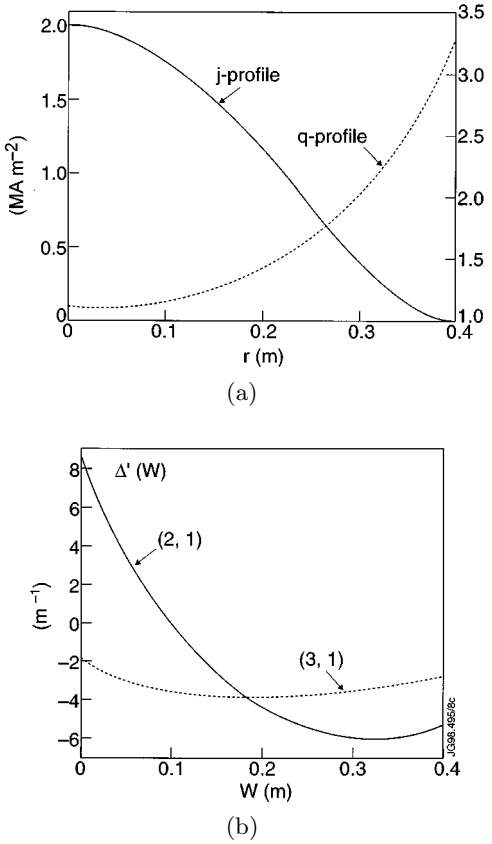

Fig. 8. (a) Current density and q-profile used in the numerical simulations. (b) Corresponding stability parameters obtained from the solution of the tearing mode equation.

5 An experimental scenario

The model presented above, is able to explain many of the features observed in Mirnov oscillations measured in Tokamak experiments. Here we show its application to the analysis of instabilities preceding disruptions observed in lower hybrid current drive (LHCD) discharges in the ASDEX Tokamak. This medium-sized machine had a major radius $R_0 = 1.65$ m, plasma column radius $a = 0.4$ m and operated at magnetic fields of up to 2.2 T. It provided during its latest operational phase useful information on the correlation between magnetic and broad-band reflectometry data [16]. The simulations presented here correspond to a discharge with a total current of 320 kA, a peaked current density profile which can be approximated by the parabolic profile shown in Figure 8, with a safety factor at magnetic axis and plasma edge $q(0) = 1.11$ and $q(a) = 3.33$ respectively and temperatures of 0.5 keV and 0.2 keV at the rational surfaces of the (2, 1) and (3, 1) modes respectively. The skin time of the vessel has the experimental value of 15 ms.

Lower-hybrid current drive discharges in ASDEX indicated that the (2, 1) tearing mode could be destabilised due to the change in the current density profile (caused by the localised power deposition of the waves), often leading to mode locking and a major plasma disruption [17].

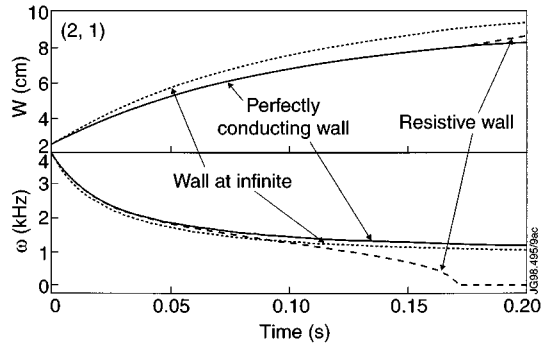

(a)

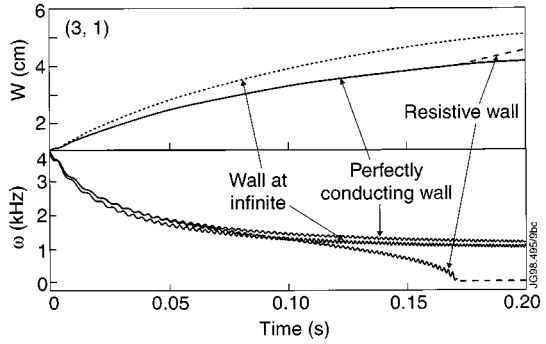

(b)

Fig. 9. Simulation with all terms included, for 3 different wall configurations. The initial input parameters are $W_2(0) = 2.5$ cm, $W_3(0) = 1$ cm, $\omega_2(0) = \omega_3(0) = 4$ kHz and $\Delta\phi(0) = 0$. The stability parameters $\Delta'_2(W)$ and $\Delta'_3(W)$ used are shown in Figure 8.

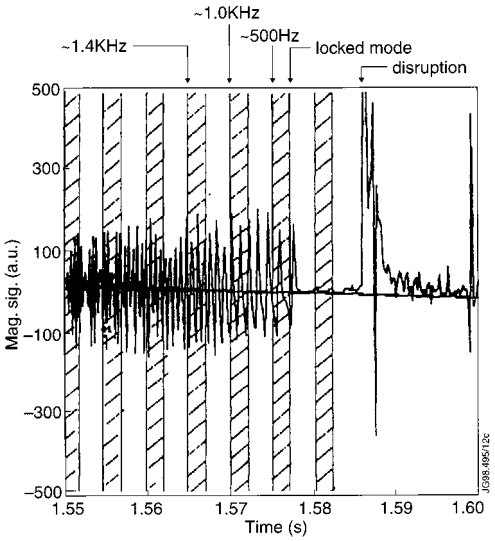

Fig. 10. Magnetic signal measured in ASDEX for discharge (#29285) showing the following MHD behaviour: at $t = 1.550$ s, a (2, 1) mode is destabilised; the mode grows rapidly and mode locking occurs at $t = 1.578$ s. A disruption occurs at $t = 1.586$ s. The dashed regions correspond to the time intervals of reflectometer measurements (sweep time of 2 ms).

In the discharge considered here, a rotating (2, 1) mode is identified from magnetic pick-up signals (see Fig. 10). Further evidence for a (2, 1) island is obtained from the analysis of microwave reflectometry corresponding to a broadband sweep operation lasting 2 ms, taken at intervals of 5 ms. The evolution of the increment of the phase during the sweep ($\Delta\Phi/\Delta F$) plotted *versus* density allows the identification of deformations in the density profiles obtained from the phase derivative through an Abel inversion (see Fig. 11). Electron density perturbations located around the $q = 2$ surface were observed both before and after mode locking ($t_{\rm lock} = 1.577$ s). Before mode locking (at $t = 1.575$ s) the observed density perturbation rotates with a frequency of 500 Hz. During mode locking (when the non-rotating (2, 1) mode is no longer detected in the magnetic signals), the phase derivative shows an abrupt increase for $n_{\rm e} = 1.2 \times 10^{19}$ m^{-3} (see Fig. 11a), indicating a sudden displacement inwards of the reflecting layers close to that density. The corresponding electron density profile (Fig. 11b) shows a plateau around the $q = 2$ surface. This indicated the presence of a (2, 1) island which grows from a width of 8 cm (at $t = 1.580$ s) until it reaches a width of ~ 10 cm before the disruption ($t_{\rm disr} = 1.587$ s). The high spatial resolution of the reflectometry diagnostic (1 cm), allows also the observation of much lower amplitude modes, sometimes undetectable in the magnetic signals. The reflectometry measurements, in Figure 11, show a small plateau around the radius of the $q = 3$ surface, possibly indicating the presence of a (3, 1) island. The latter is only observed after locking of the (2, 1) island, and given the time resolution of the diagnostic, it is not possible to say the precise time when it became unstable or what is its initial evolution. Reflectometry measurements show however that the disruption occurs soon after the (2, 1) and (3, 1) islands have grown large enough to overlap. Another interesting observation is that locking for both modes has not occurred simultaneously. Reflectometry measurements taken after the (2, 1) mode has locked, indicate that the (3, 1) mode is still either rotating or oscillating for at least another 5 ms.

The results of simulations are shown in Figure 12. These are not intended to reproduce the experimental observation in detail, but rather to show that the non-linear model presented above is able to explain many of the observed characteristics. The calculated evolution of the amplitude and frequency of the $m = 2$, $n = 1$ mode up to the time of locking is consistent with the observed one. The simulation shows that after the $m = 2$ island locks, the $m = 3$ will continue to oscillate for another 5 ms (Fig. 12b), in agreement with the observations made with reflectometer data. After the locking of both islands, further growth of the modes leads to island overlap on a time scale that agrees also with the time when ASDEX disruptions were observed ($\sim$ 10 ms after the locking). This realistic example further illustrates that the toroidal coupling between the (2, 1) and (3, 1) islands strongly affects the amplitude and rotation of the outer (3, 1) island. Notice that although the frequencies are initially different, the two modes soon start to rotate with the frequency

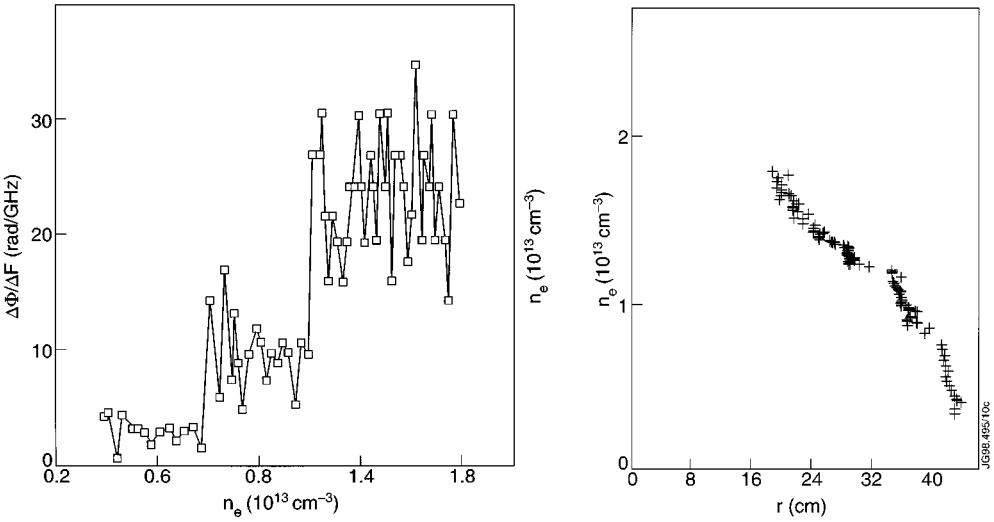

Fig. 11. Results from broad-band reflectometry obtained in the ASDEX Tokamak for discharge 29285, at $t = 1.58$ ms, when locking of the $m = 2$, $n = 1$ mode occurred. The abrupt jumps in the phase derivative $\Delta\phi/\Delta F$ (a) correspond to the flattening of the plasma density in the evaluated density profiles (b), revealing the influence of magnetic islands located near the rational surfaces $q = 2$ ($r \sim 30$ cm) and $q = 3$ ($r \sim 39$ cm).

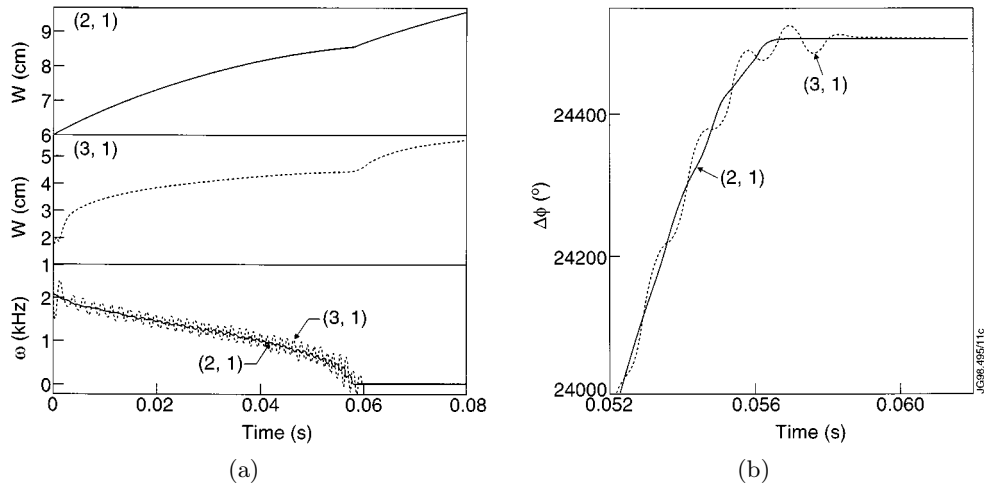

Fig. 12. Simulation of (2, 1) and (3, 1) islands observed in an ASDEX discharge before a disruption. The following input parameters were used: $W_2(0) = 6.0$ cm, $W_3(0) = 1.5$ cm, $\omega_2(0) = 2.2$ kHz, $\omega_3(0) = 1.7$ kHz, $f_2 = f_3 = 0$, with $\Delta'_2(W) > 0$ and $\Delta'_3(W) < 0$ shown in Figure 8. (a) Plots of W and ω as a function of time; (b) plot of the phases as a function of time around the time of locking. The $m = 3$, $n = 1$ mode continues to oscillate after the locking of the $m = 2$, $n = 1$ mode.

of the larger (2, 1) mode. Each island rotates, as well as oscillates in the potential of the other.

6 Conclusions

On the basis of tearing mode theory we have developed a relatively simple and physically explicit model of the evolution of toroidally coupled rotating magnetic islands. The basic mechanism identified by the model in the island evolution is the locking in phase of rotating islands on one another, that leads to rapid destabilisation of an initially stable mode ($\Delta'(0) \leq 0$). The island growth is governed by the phase dependent coupling term, on its turn dependent on the eddy currents induced in the resistive wall, which cause also the known slowing of the rotation [14].

The combined effects of coupling, wall and inertia can compete and overcome other intrinsic destabilising effects, not included here, as for instance a neo-classical driving term ($\alpha\beta_p$) [18], possibly explaining observations of larger than expected $m = 3$ islands in low β_p discharges in the JET Tokamak [19]. In addition, in this work,

for the purpose of isolating and understanding the role of the electrodynamic coupling mechanism, the drag on the *toroidal* motion due to perpendicular viscosity has been neglected. Viscosity would not alter the phase space topology of the dynamic system studied here, but only the time scales. Viscosity is important when the two interacting islands are sufficiently close to each other. Then the viscous torques can make the plasma "trapped" inside both islands to rotate with the same toroidal velocity. As it was shown in the examples in Sections 4 and 5, coupling leads to phase-locking with a phase-difference which in general it is destabilising. A viscous layer ultimately produces a modification in the effective toroidal moment of inertia of the island, and introduces a further destabilising phase shift between two islands. The viscous layer around each island provides smooth velocity gradients around each island and thus, allows for the inertial effect related to the island growth considered in this paper.

It is important to consider the role of mode coupling in the schemes of feedback control of the tearing instabilities. The analytic expressions for the electromagnetic torque and modification to the stability parameter presented in the dynamic system given in equations (19–22), can be easily included in existent work on feedback stabilisation. This system of equations was obtained in the "tenuous" plasma limit, which is an appropriate approximation for MHD modes located in the outer regions of a Tokamak plasma.

Several simulations were presented which illustrate the individual role of coupling, plasma inertia and resistive vessel in the non-linear stability of $m = 2$ and $m = 3$ modes with toroidal number $n = 1$. For realistic Tokamak parameters we find that an initially small and stable $m = 3$ island, with an island size of the order of the ion Larmor radius, could grow to a size comparable to a much larger $m = 2$ island, say $W_2/a = 0.2$, in a few hundred milliseconds. It is also possible to obtain solutions where W_3 would become larger than W_2. (In the examples solved for Fig. 2, smaller changes in the current density equilibrium profile could lead to such solutions.) In practice, island overlapping is likely to lead to disruption before that could be observed.

In the examples shown in Figures 2a and 2b, where rotation was neglected, given the appropriate phase, an $m = 3$ island is always unstable independent of the initial size of the driving $m = 2$ island. In a more general case, with the resistive wall included, non-linear $m = 3$ growth occurs only for W_2/W_3 above a certain threshold value. In order to get mode destabilisation by coupling, phase lock between the modes must be achieved. In the limits of no wall or $\omega \to 0$ and of a perfectly conducting wall or $\omega\tau_{\rm wall} \gg 0$ coupling leads to locking of the phases with an average phase difference $\Delta\phi = 0$. In general, phase locking may also occur for $\Delta\phi \neq 0$.

Previous studies on the effect of a resistive wall indicated that rotation is stabilising [11], it should be noted that with mode coupling this is not always true. The example in Figure 7 shows that at least transiently it is possible to obtain solutions where a mode remains stable in spite of the frequency being decreased.

The model was applied to the interpretation of MHD observations in LHCD discharges made on ASDEX. The calculated evolution of the island widths and frequencies were found to be consistent with the evolution of (2, 1) and (3, 1) modes preceding a disruption as observed with the magnetic and density reflectometer diagnostics.

We would like to thank Dr. H. Zohm for fruitful discussions and for providing the relevant magnetic data from ASDEX. We also like to acknowledge useful discussions with Dr. P. Savrukhin. We are grateful to Miss I. Nunes for simulations of tearing mode stability.

References

1. B.A. Carreras, IEEE Trans. Plasma Sci. **25**, 1281 (1997); R.J. Buttery *et al.*, *Proc. 26th E.P.S. Conf. Controlled Fusion and Plasma Physics*, Maastricht, 14-18 June 1999, European Physical Society, ECA, Vol. 23J, pp. 121-124.
2. J.W. Connor, S.C. Cowley, R.J. Hastie, T.C. Hender, A. Hood, T.J. Martin, Phys. Fluids **31**, 577 (1988).
3. R. Fitzpatrick, R.J. Hastie, T.J. Martin, C.M. Roach, Nucl. Fusion **33**, 1533 (1993).
4. A.B. Mikhailovskii *et al.*, Plasma Phys. Rep. **23**, 844 (1997).
5. B. Carreras, H.R. Hicks, D.K. Lee, Phys. Fluids **24**, 66 (1981).
6. E. Lazzaro, M.F.F. Nave, Phys. Fluids **31**, 1623 (1988).
7. R. Fitzpatrick, Nucl. Fusion **33**, 1049 (1993).
8. A.I. Smolyakov, E. Lazzaro, A.I. Hirose, G. Re, J.D. Callen, Phys. Plasmas **2**, 1581 (1995).
9. G. Bosia, E. Lazzaro, Nucl. Fusion **6**, 1003 (1991).
10. R. Fitzpatrick, C. Gimblett, R.J. Hastie, *Proc. 20th E.P.S. Conf. Controlled Fusion and Plasma Physics*, Lisbon, 26-30 July 1993, European Physical Society, Contributed Papers, Vol. 17C, part IV, p. 1335.
11. P.H. Rutherford, Phys. Fluids **16**, 1903 (1973).
12. H. Strauss, Phys. Fluids **19**, 134 (1976).
13. S. Hirshman, D.J. Sigmar, Nucl. Fusion **21**, 1079 (1981).
14. M.F.F. Nave, J.A. Wesson, Nucl. Fusion **30**, 2575 (1990).
15. M. Kikuchi, Nucl. Fusion **26**, 101 (1986).
16. M.E. Manso, A. Silva, F. Serra, J. Matias, J. Mendonça, *Proc. 17th EPS Conf. on Contr. Fusion and Plasma Heating*, Amsterdam, 25-29 June 1990, European Physical Society, Contributed papers, Vol. 14 B, part II, p. 837.
17. H. Zohm, F. Söldner, H. Bruhns, R. Büchse, F. Leuterer and the ASDEX Team, Plasma Phys. Contr. Fusion **33**, 1423 (1991).
18. H. Zohm *et al.*, Plasma Phys. Contr. Fusion **39**, B237 (1997).
19. M.F.F. Nave, A.W. Edwards, K. Hirsch, M. Hugon, A. Jacchia, E. Lazzaro, H. Salzmann, P. Smeulders, Nucl. Fusion **32**, 825 (1992).